Research article

MEDAG expression in vitro and paeoniflorin alleviates bone loss by regulating the MEDAG/AMPK/PPARγ signaling pathway *in vivo*

Haixia Liu [a,1], Zhiyue Chang [b,1], Shuling Liu [c], Ruyuan Zhu [a], Jiayi Ma [a], Xinyue Lu [a], Lei Li [c,*], Zhiguo Zhang [a,**]

[a] *Institute of Basic Theory for Chinese Medicine, China Academy of Chinese Medical Sciences, Beijing, China*
[b] *The 8th Medical Center, Chinese PLA General Hospital, Beijing, China*
[c] *Dongzhimen Hospital, Beijing University of Chinese Medicine, Beijing, China*

A R T I C L E   I N F O

A B S T R A C T

Objectives: Osteoporosis (OP) is characterized by reduced bone mass and impaired bone microstructure. Paeoniflorin (PF) is isolated from peony root with anti-inflammatory, immunomodulatory, and bone-protective effects. Up to now, the mechanism of anti-OP in PF has not been completely clarified.
Methods: The expression of MEDAG in osteoclasts, osteoblasts and adipocytes was detected by RT-qPCR. The OVX mouse model was constructed, and oral administration of PF was performed for 15 weeks. Bone microstructure was detected by H&E staining and a micro-CT system, and expression of signaling proteins examined by Western blot and immunohistochemical staining. ELISA and biochemical kits were used to quantify serum metabolite levels.
Key findings: MEDAG were upregulated in osteoclasts and adipocytes, and downregulated in osteoblasts. PF administration effectively alleviated OVX-induced bone loss, and histological changes in femur tissues. Moreover, PF significantly reduced serum TRAP, CTX-1, P1NP, BALP, and LDL-C levels and increased HDL-C. In addition, PF inhibited the expression of MEDAG, cathepsin K, NFATc1, PPARγ, and C/EBPα and increased *p*-AMPKα, OPG and Runx2.
Conclusions: MEDAG is a potential target for bone diseases, and PF might attenuate OVX-induced osteoporosis via MEDAG/AMPK/PPARγ signaling pathway.

1. Introduction

Osteoporosis (OP) is a common degenerative disease in which the bone mass is reduced and the bone microstructure is destroyed, resulting in an increase in bone fragility and a susceptibility to fracture [1]. During menopause, there is a loss of ovarian function, leading to decreased estrogen levels. Estrogen deficiency not only affects the imbalance of bone resorption of osteoclasts and bone formation of osteoblasts but also exerts lipid metabolic disorders. After menopause, estrogen deficiency mediates changes in body fat distribution and body composition by increasing visceral fat [2].

Recently, mesenteric estrogen-dependent adipogenesis (MEDAG), also called Meda-4, has been identified to contribute to the

differentiation and metabolism of adipocytes, which is beneficial for preadipocyte differentiation, the content of lipid droplets and glucose uptake in adipocytes [3]. MEDAG expression decreases with increased estrogen concentration in adipocytes, and estrogen supplementation can reduce the elevated expression of MEDAG in the fat tissues of ovariectomized (OVX) mice [3]. MEDAG is also upregulated in osteoarthritis and diabetes [4,5]. Therefore, the relationship between MEDAG and OP is of interest.

Furthermore, MEDAG can not only regulate the AMP-dependent protein kinase (AMPK)/mTOR pathway [6], but is an upstream regulator of peroxisome proliferation-activated receptors γ (PPARγ) [3,7]. There is increasing evidence that AMPK can regulate PPARγ expression [8], which is a master regulator of adipocyte development, and adipocyte production requires a basal level of AMPK [9]. Moreover, bone loss caused by PPARγ agonist pioglitazone in diabetic rats can be improved through AMPK activation pathway [10]. PPARγ activation supports osteoclast differentiation [11] and leads to bone loss and bone marrow fat accumulation, while low expression of osteocyte specific PPARγ causes an increase in bone mass and a reduction in bone marrow fat [12]. PPARγ shRNA also increases osteoblast differentiation and inhibits adipocyte generation [13]. Therefore, as a regulator of AMPK and PPARγ, MEDAG may have a certain role in all three types of cells and OP.

Paeoniflorin (PF) is isolated from peony root including *Paeonia lactiflora* Pall. and *Paeonia suffruticosa* Andr. in Ranunculaceae, which has anti-inflammatory and bone-protective effects [14,15]. PF is an effective component of Liuwei Dihuang Decoction, which has anti-osteoporosis effect [16,17]. As a glycoside, PF is from *Paeonia lactiflora* Pall. and found increases osteoblast differentiation [18]. In hyperlipidemia-induced OP rats, PF has the effect of reducing total cholesterol (TC), triglycerides (TG), and low-density li-poprotein cholesterol (LDL-C) and improve bone trabecular and cortical parameters [15]. PF suppressed osteoclastogenesis and facilitated osteoblastogenesis by manipulating NF-κB actions, Wnt/β-catenin and AKT/mTOR signaling pathway [19–21].

Therefore, the aim of this study was to study the expression of MEDAG in osteoclasts, osteoblasts and adipocytes, and PF attenuated bone loss via the MEDAG/AMPK/PPARγ signaling pathway. OVX mice were administered with PF to explore its effects on serum bone and lipid metabolism-related expressions, bone mineral density, and markers of osteoclasts, osteoblasts and adipocytes.

2. Materials and methods

2.1. Materials

RAW264.7 cells were purchased from Cell Resource Center, Peking Union Medical College (Beijing, China). Human adipose-derived stem cells (hADSCs) were donated from School of Basic Medicine Peking Union Medical College. RANKL (462-TEC-010) was were supplied by R&D Systems (Minneapolis, MN, USA). β-glycerophosphate disodium salt hydrate (G9422), ʟ-ascorbic acid (A4544), dexamethasone (D4902), 3-isobutyl-1-methylxanthine (I5879) were bought from Sigma Aldrich Inc. (Merck KGaA, Germany). PF was bought from Nanjing Dilger Medical Technology (CAS: 23180-57-6; purity >98 %). Enzyme-linked immunosorbent assay (ELISA) kits for P1NP (QS47784), CTX-1 (QS47767), BALP (QS440290), and TRAP (QS440351) were obtained from Beijing gersion Bio-Technology Co., Ltd. HDL-C (A112-1-1) and LDL-C (A113-1-1) kits were purchased from Nanjing Jiancheng Bioengineering Institute (Nanjing, China). NFATc1 (66963-1-Ig), cathepsin K (11239-1-AP), C/EBPα (18311-1-AP), and PPARγ (16643-1-AP) antibodies were purchased from Proteintech Group (Hubei China). MEDAG (orb326838) antibody was purchased from biorbyt (UK). Phospho (p)-AMPKα (Thr172) (2535S) antibody was purchased from Cell Signaling Technology (Danvers, MA, USA). Runx2 (ab236639) and OPG (ab73400) antibodies were purchased from Abcam (Cambridge, UK).

2.2. Cell culture and differentiation

RAW264.7 cells were cultured in DMEM containing 10 % FBS, and incubated in a humidified incubator at 37 °C with 5 % CO_2. RAW264.7 cells were seeded on 24 well plates, attached to the wall, and exposed to RANKL (50 ng/ml) for osteoclast differentiation. Cells were collected at different time-points (0, 3, 5 days).

hADSCs were cultured in DMEM/F12 supplemented with 10 % FBS, and incubated in a humidified incubator at 37 °C with 5 % CO_2. hADSCs were seeded on 24 well plates, attached to the wall, and exposed to β-glycerophosphate disodium salt hydrate (10 mM) and ʟ-ascorbic acid (50 μg/ml) for osteoblast differentiation, and dexamethasone (1 μM), 3-isobutyl-1-methylxanthine (100 μg/ml) and ʟ-ascorbic acid (50 μg/ml) for adipocyte differentiation. Cells were collected at different time-points (0, 3, 5, 7 days).

2.3. Animal experiments

Forty female C57BL/6J mice (9–10 weeks old, 17–20 g), from Beijing Vital River Laboratory Animal Technology Co., Ltd. [certification number SCXK (Jing) 2021-0006], were used for this study. Mice were housed in SPF conditions [certification number SYXK (Jing) 2021-0017] at the Institute of Basic Theory, China Academy of Chinese Medical Sciences at 21–23 °C and humidity of 50–60 % in a 12-h light/dark cycle. All animals were allowed free access to water and a standard diet. The experiments were approved by the Institutional Ethics Committee of the China Academy of Chinese Medical Sciences.

After one week of acclimation, the mice were anesthetized by injection with 1 % pentobarbital sodium (i.p., 4 ml/kg) and then received bilaterally OVX or sham operation (Sham). Ten days after surgery, OVX mice were randomly divided into three groups: OVX group (n = 10), estradiol valerate (EV) group (n = 10), and PF group (n = 10). The mice in the Sham and OVX groups received distilled water by gavage. The mice in the EV and PF groups were administered 0.13 mg/kg EV and 50 mg/kg PF daily by gavage. Dose of 50 mg/kg PF has been shown to be effective in a number of animal models [22]. In addition, treatment with 20 or 30 mg/kg PF administered by gavage can prevent bone loss in rats [15,23]. Therefore, we choose 50 mg/kg PF for the mice. After 15 weeks of

Table 1
List of primer sequences.

Gene Names	Forward primer sequence (5'–3')	Reverse primer sequence (5'–3')
MEDAG (mice)	GGCCTTGTGCGCCTAGAAG	TGCTCAGTATCGTTTCCCTGTA
TRAP (mice)	GTCAAGAACTTGCGACCATTG	CGTTCTCGTCCTGAAGATACTG
β-actin (mice)	TTTCCAGCCTTCCTTCTTGG	GGCATAGAGGTCTTTACGGATG
MEDAG (human)	TCTGCCACCCTGAACATTT	GAGGGCCAAACCCTGATTTA
C/EBPα (human)	AAGCACGATCAGTCCATCC	GCACAGAGGCCAGATACAA
β-actin (human)	TCCACGAAACTACCTTCAACTC	CAGTGATCTCCTTCTGCATCC

treatment, mice were sacrificed, and their body weight and body length were recorded to calculate Lee'S index by the following formula: [body weight $(g)^{1/3} \times 1000$]/body length (cm). Femurs and tibias were removed for hematoxylin-eosin (H&E) staining, micro-CT analyses, Western blot and immunohistochemical (IHC) analysis, and serum samples were taken for ELISA and biochemical analysis.

2.4. ELISA and biochemical analysis

The levels of P1NP, CTX-1, BALP, TRAP, HDL-C, and LDL-C from mouse serum were assessed using the corresponding ELISA and biochemical kits, and all procedures were subject to the manufacturer's instructions.

2.5. Micro-CT analysis

The femurs were scanned at 6.5 μm resolution for quantitative analysis using a micro-CT system Skyscan1276 (Bruker, Kartuizersweg, Belgium). Using the lowest point of the femoral growth plate as the baseline, set the area of 1 mm thickness as the area of interest (ROI) for three-dimensional reconstruction. The three-dimensional image was reconstructed with N-Recon software, and the trabecular bone distribution and BMD were detected with CT-AN software.

2.6. Histological staining

Femurs were fixed in 4 % paraformaldehyde and decalcified in 10 % EDTA, then the specimens were embedded in paraffin and sectioned at 4 μm. Paraffin sections were used for H&E staining according to the kit protocol. Images were captured by a Leica Aperio VERSA 8 scanner (Leica Biosystems, Germany).

2.7. IHC analysis

After dewaxing and hydration, sections were incubated with antigen retrieval solution and 3 % H_2O_2 and permeated with 0.04 % TritonX-100. After washing, the sections were blocked with 10 % goat serum for 30min and incubated overnight with primary antibodies against MEDAG (1:200), Runx2 (1:50), and OPG (1:400) at 4 °C. The sections were incubated with corresponding secondary antibodies for 30min, and then stained by DAB and hematoxylin. The images were acquired with a Leica Aperio VERSA 8 scanner (Leica Biosystems, Germany).

2.8. Western blot analysis

Under low-temperature conditions of liquid nitrogen, the tibias were pulverized, then extracted with lysis buffer (Beyotime, Shanghai, China). Protein samples (50 μg) were loaded into an SDS-PAGE gel, separated by electrophoresis, and then transferred to a PVDF membrane. After blocking, the membrane was incubated with primary antibodies against MEDAG (1:500), *p*-AMPKα (1:1000), PPARγ (1:1000), C/EBPα (1:1000), cathepsin K (1:1000), NFATc1 (1:1000) and GAPDH (1:2000) at 4 °C overnight and then with the corresponding secondary antibody. Protein expression was visualized on a chemiluminescence system and quantified using Image J software.

2.9. Quantitative real-time polymerase chain reaction (RT-qPCR)

Total RNA from cells was isolated with Trizol reagent (Takara Bio, Tokyo, Japan), and was reverse-transcribed to obtain cDNA. cDNA was added to the PR-qPCR reaction system for amplification. The $2^{-\Delta\Delta Ct}$ method was used to calculate the relative gene expression, and β-actin was measured as an internal control. The primers are shown in Table 1.

2.10. Statistics

The data are presented as mean ± SD. All data were performed using GraphPad Prism 5 (GraphPad, Diego, USA). Two-tailed Student's t-tests were used to compare two groups, and one-way ANOVA was used to compare more than two groups. The
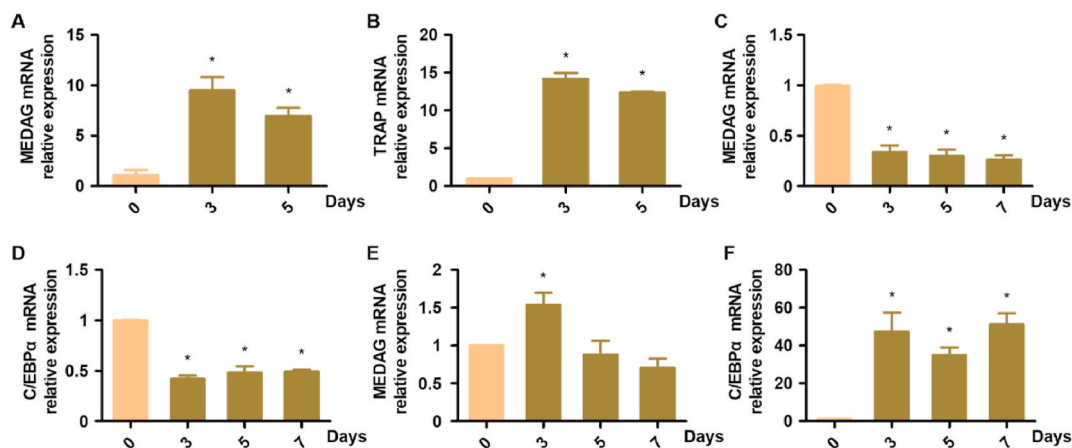
Fig. 1. MEDAG expression in osteoclasts, osteoblasts and adipocytes. RT-qPCR results showed that (A) MEDAG and (B) TRAP mRNA expression in RAW264.7 cells differentiated into osteoclasts on days 0, 3, 5. (C) MEDAG and (D) C/EBPα mRNA expression in hADSCs differentiated into osteoblasts on days 0, 3, 5, 7. (E) MEDAG and (F) C/EBPα mRNA expression in hADSCs differentiated into adipocytes on days 0, 3, 5, 7. Compared with the day 0 (*p < 0.05).
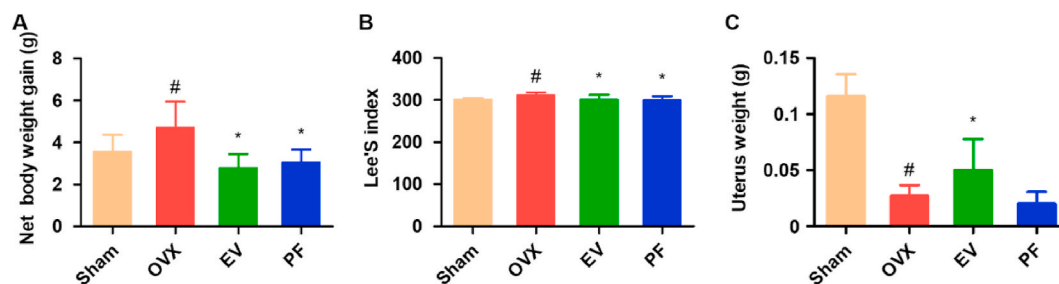
Fig. 2. PF preserved ovariectomized (OVX)-induced body weight, fat gain, and uterus atrophy in OVX mice. (A) Net body weight gain (B) Lee'S index, and (C) Uterus weight and in different groups of mice. Compared with OVX group (*p < 0.05) and compared with Sham group (#p < 0.05).

definition of statistical significance was p < 0.05.

3. Results

3.1. MEDAG expression in osteoclasts, osteoblasts and adipocytes

RAW 264.7 cells could differentiate into osteoclasts after adding osteoclast induction medium. RNA samples were collected on days 0, 3, 5 after osteoclast differentiation induction, and the expression of MEDAG and osteoclast marker gene TRAP were detected by RT-qPCR method. In osteoclasts, the expression of MEDAG and TRAP was elevated (Fig. 1A and B). These results indicated that the expression of MEDAG in osteoclast was elevated.

hADSCs could differentiate into osteoblasts and adipocytes. In osteoblasts, as shown in Fig. 1C and D, MEDAG and C/EBPα were downregulated and not significantly different with the induction time of osteogenesis. The results showed that MEDAG was down-regulated in osteoblasts. In addition, in adipocytes, as shown in Fig. 1E and F, MEDAG was upregulated on day 3 and was not significantly different on days 5 and 7, and C/EBPα was upregulated. It was found that the up-regulated expression of MEDAG in adipocytes was time-sensitive.

3.2. PF alleviated body weight and fat gain without uterotrophic effects

Body weight, fat gain and uterus atrophy were observed in OVX mice. As displayed in Fig. 2A and B, OVX mice had a significant increase in net body weight gain compared with Sham mice. Notably, PF treatment significantly inhibited net body weight gain. In addition, compared to the Sham group, the OVX group had an increased Lee's index, which can be used to evaluate the total body fat percentage. Interestingly, EV and PF administration significantly prevented these alterations. As expected, OVX resulted in uterine atrophy, and EV administration but not PF to OVX mice significantly increase uterus weight (Fig. 2C).
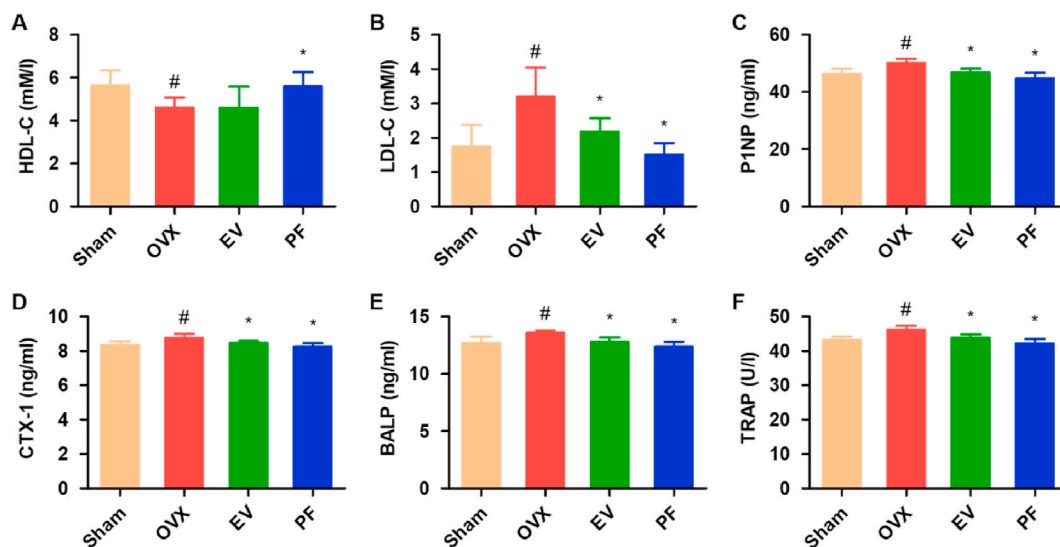
Fig. 3. PF improved HDL-C, LDL-C, P1NP, CTX-1, BALP, and TRAP in OVX mice. (A) HDL-C, (B) LDL-C, (C) P1NP, (D) CTX-1, (E) BALP, and (F) TRAP in different groups of mice. Compared with OVX group (*p < 0.05) and compared with Sham group (#p < 0.05).
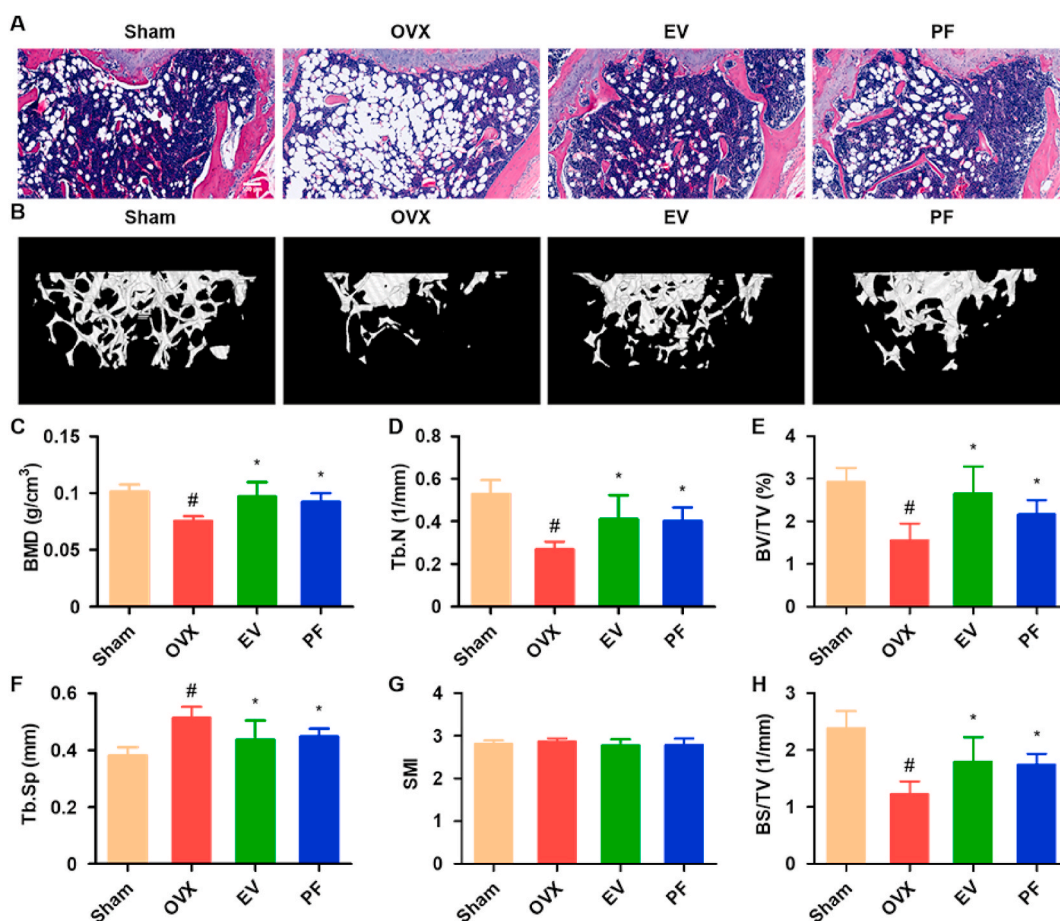
Fig. 4. PF improved bone microstructure in OVX mice. (A) H&E staining observed under a microscope (the original magnification is × 200) (B) Bone microstructure scan image, and its analysis parameters including (C) BMD, (D) Tb.N, (E) BV/TV, (F) Tb.Sp, (G) SMI, and (H) BS/TV in different groups of mice. Compared with OVX group (*p < 0.05) and compared with Sham group (#p < 0.05).
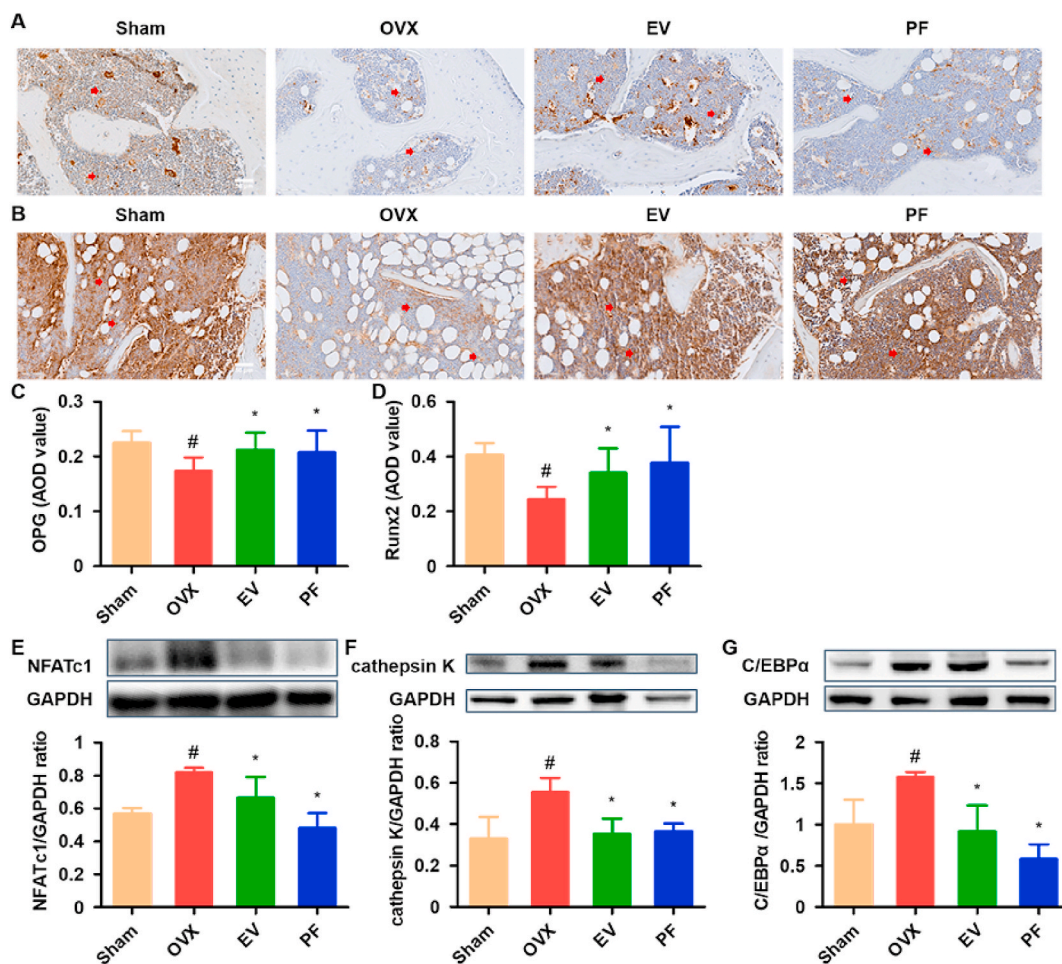
Fig. 5. PF increased OPG and Runx2 expression and decreased cathepsin K, NFATc1, and C/EBPα expression in OVX mice. IHC staining the expression of (A & C) OPG and (B & D) Runx2 observed under a microscope (the original magnification is × 400, scale bar = 50 μm), red arrows indicated positive expression and its AOD value in mice femurs. The expression of (E) NFATc1, (F) cathepsin K, and (G) C/EBPα in mice tibias were detected by Western blot. Compared with OVX group (*p < 0.05) and compared with Sham group (#p < 0.05). (For interpretation of the references to colour in this figure legend, the reader is referred to the Web version of this article.)

3.3. PF decreased LDL-C, P1NP, CTX-1, BALP, and TRAP and increased HDL-C

As illustrated in Fig. 3A–F, the levels of LDL-C, P1NP, CTX-1, BALP, and TRAP were significantly increased, and HDL-C was decreased after OVX. Compared with OVX group, EV and PF treatment significantly reversed these alterations. However, HDL-C level did not increase after EV treatment. Taken together, it is indicated that PF could inhibit dyslipidemia and bone high turnover.

3.4. PF improved bone microstructure alterations

As revealed in Fig. 4A, H&E staining demonstrated that compared to the Sham group, the OVX group has fewer bone trabeculae and more fat droplets in the femur. Interestingly, supplementation of EV and PF to OVX mice significantly increased bone trabeculae and decreased fat droplets.

As displayed in Fig. 4B, compared with Sham group mice, the OVX group mice showed bone loss, sparse and disordered arrangement of bone trabeculae, and osteoporotic changes in bone microstructure; After intervention, the formation of bone in mice increased, the arrangement of bone trabeculae was tight, regular, and the bone microstructure improved. As shown in Fig. 4C–H, bone mineral density (BMD), trabecular number (Tb.N), percent bone volume (BV/TV), and bone surface density (BS/TV) were significantly lower in the OVX group than in the Sham group, while trabeculae dissociation (Tb.Sp) was significantly higher. As expected, these parameters were normalized by EV and PF supplementation.
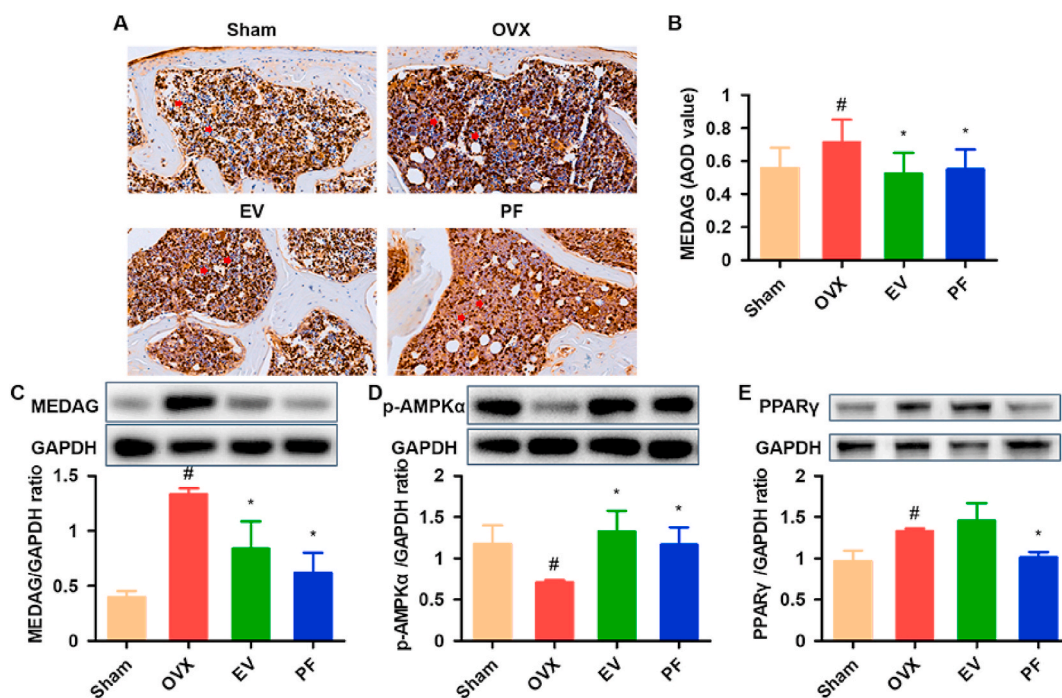
Fig. 6. PF improved MEDAG/AMPK/PPARγ pathway in OVX mice. IHC staining the expression of (A) MEDAG observed under a microscope (the original magnification is × 400, scale bar = 50 μm), red arrows indicated positive expression and its AOD value (B) in mice femurs. The expression of (C) MEDAG, (D) *p*-AMPK, and (E) PPARγ in mice tibias were detected by Western blot. Compared with OVX group (*p < 0.05) and compared with Sham group (#p < 0.05). (For interpretation of the references to colour in this figure legend, the reader is referred to the Web version of this article.)

3.5. PF increased OPG and Runx2 expression and decreased cathepsin K, NFATc1, and C/EBPα expression

Next, markers of osteoblasts, osteoclasts and adipocytes were detected by Western blot and IHC. As illustrated in Fig. 5A–G, OVX mice showed a significant reduction in OPG and Runx2 in comparison with Sham mice, while NFATc1, cathepsin K and C/EBPα were elevated. PF treatment of OVX mice significantly decreased NFATc1, cathepsin K and C/EBPα expression and increased OPG and Runx2 expression.

3.6. Effects of PF on MEDAG/AMPK/PPARγ pathway in OVX mice

As shown in Fig. 6A–E, MEDAG and PPARγ were higher than those in Sham mice, whereas *p*-AMPK was decreased. These effects could be ameliorated by PF treatment, indicating that OVX induced abnormality in the MEDAG/AMPK/PPARγ pathway, whereas PF supplementation could improve the MEDAG/AMPK/PPARγ pathway in OVX mice.

4. Discussion

In this study, we show that MEDAG is highly expressed in osteoclasts, adipocytes and OVX mice, while low in osteoblasts. PF treatment alleviated OVX-induced body weight and fat gain without uterotrophic effects, reversed bone loss, and restored bone microarchitecture, as well as improved dyslipidemia. Moreover, PF decreased the expression of LDL-C, P1NP, CTX-1, BALP, TRAP, cathepsin K, NFATc1, C/EBPα, MEDAG, and PPARγ, and increased the expression of HDL-C, OPG, Runx2 and *p*-AMPK in OVX mice.

PF, derived from Peony, was developed successfully to help improve menopause [24]. PF also restored bone microarchitecture which is in line with a previous study [25], suggesting that PF has a bone protective effect. PF reduced BMD by inhibiting the formation of osteoclasts and resorptions [26]. It is reported that PF can reduce osteopenia in mice by speeding up mineralization and bone formation [21]. PF treatment affects fat metabolism and increases in glycerol release [27]. Furthermore, the influence of PF on bone mass in post-menopausal OP mice was investigated in OVX-induced mice [19]. Paeoniflorin not only has a protective effect on osteoporosis induced by estrogen deficiency, but also has an effective effect on other types of osteoporosis. Studies found PF alleviate dexamethasone-induced osteoporosis by promoting osteogenic differentiation and autophagy [21], and high-carbohydrate, high-fat diet-induced osteoporosis by controlling the serum lipid profile and promoting osteoblasts differentiation [15].

A growing number of experiments have proved that PF can inhibit osteoclast and adipocytes, and promote the function of osteoblasts. NFATc1 and cathepsin K are osteoclast-specific genes, OPG and Runx2 are osteoblast differentiation-regulators, and PPARγ and C/EBPα are important factors in the differentiation of adipocytes. Indeed, in our study, PF has been shown to prevent bone loss
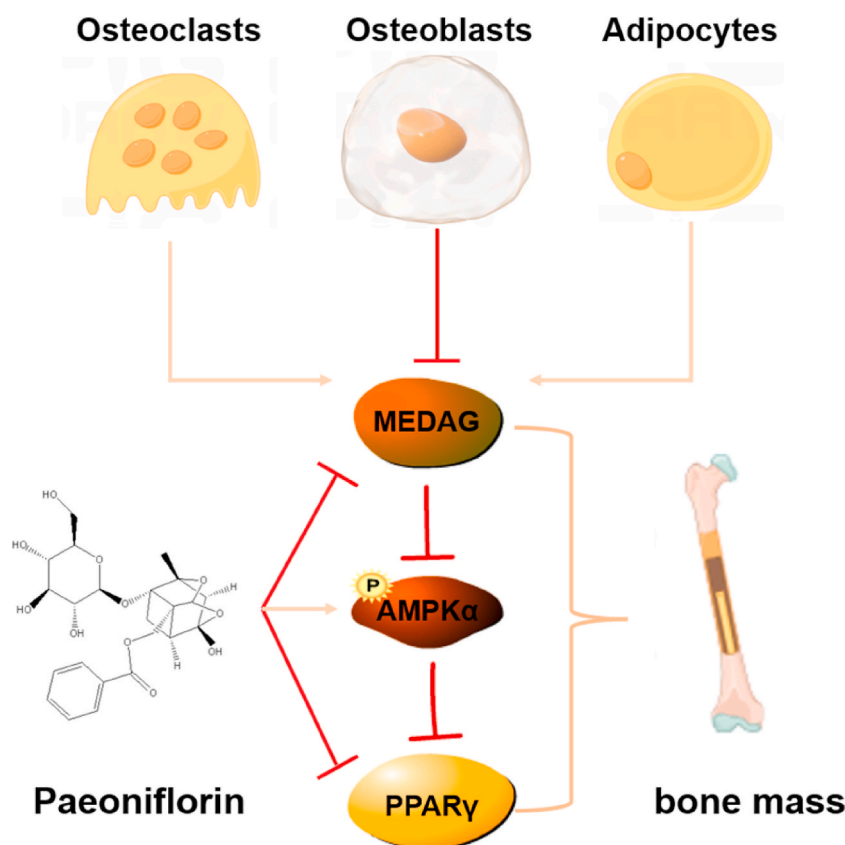
Fig. 7. Schematic diagram of MEDAG expression and the underlying mechanism of paeoniflorin (PF) against osteoporosis in ovariectomized mice. MEDAG expression increases in osteoclasts and adipocytes, but decreases in osteoblasts. PF inhibits MEDAG and PPARγexpression and increases *p*-AMPKαexpression, thereby increasing bone mass. The arrow sign (↓) means promoting. The stop sign (⊥) means inhibiting.

caused by OVX-induced bone loss by enhancing bone formation and reducing bone resorption and adipocytes, as illustrated in Figs. 5 and 6.

Dyslipidemia is closely related to OP, with OP occurring in high-fat animals, and hyperlipidemia inhibits bone marrow stromal cell spreading and osteoblastogenesis [15]. Lower HDL and higher LDL levels are related to increased risk of OP in postmenopausal women [28]. HDL-C disturbance benefits adipocyte differentiation and inhibits osteoblast differentiation [29]. Moreover, statins have a protective effect on bone via decreasing LDL-C to increase BMD [30]. Previously, we reported lower HDL-C and higher LDL-C levels in OVX-induced OP rats [31]. Treatment with PF reduced LDL-C and elevated HDL-C in OVX mice. In support of the current findings, PF reduced LDL-C and elevated HDL-C in hyperlipidemia rats [15].

It is the first time that the expression of MEDAG in osteoclasts, osteoblasts, adipocytes and bone tissues has been demonstrated. Our result show that MEDAG is expressed differently in different cells and localized to the cytoplasm in bone slices. MEDAG is expressed in undifferentiated 3T3-L1 cells and increases during differentiation, indicating its involvement in adipogenesis [3]. Our research found that MEDAG involvement in osteogenesis and osteogenesis, as well as adipogenesis. However, unlike previous studies, MEDAG did not increase with adipocyte differentiation time, possibly due to differences in cells and differentiation conditions. MEDAG is believed to play a key role in the onset and progression of the disease [3,6] and OVX increases MEDAG expression [3]. The present study confirmed that OVX induced high MEDAG expression in mouse bone tissues, whereas EV and PF supplementation reduced MEDAG levels.

AMPK, a regulator of energy homeostasis, is widely expressed, including in bone. Activation of AMPK regulates bone formation and maintenance of bone mass *in vivo*, and its phosphorylation can enhance osteoblast function and inhibit osteoclast and adipocyte function [32–34]. AMPK deletion in osteoblasts reduces osteoblast differentiation and enhances osteoclast number [9]. Our results demonstrated that OVX could induce bone loss as evidenced by inhibiting *p*-AMPK, whereas PF supplement could inhibit bone loss via increasing *p*-AMPK expression in OVX mice.

It has been shown that MEDAG plays an important role in lipid metabolism, and PPARγ regulation [3]. PPARγ regulates mesenchymal cells to osteoblasts and adipocytes, and as well as osteoclast recruitment. PPARγ is beneficial for the differentiation of mesenchymal cells into adipocytes instead of osteoblasts [35], and PPARγ-deficiency in mesenchymal cells increases bone mass [36]. In addition, PPARγ regulates bone formation and bone resorption [11]. In this study, PF treatment for 15 weeks decreased PPARγ protein levels in OVX mice, suggesting that bone-protective effect of PF in OVX mice might be related to PPARγ inhibition.

5. Conclusion

In conclusion, we show the expression of MEDAG in bone homeostasis related cells and osteoporosis for the first time, and treatment with PF improves bone loss and lipid profiles in OVX mice through MEDAG/AMPK/PPARγ signaling pathway by decreasing MEDAG and PPARγ expression and increasing *p*-AMPK expression (Fig. 7).

Data availability statement

Data will be made available on request.

Ethics statement

All procedures were performed in accordance with the guidelines approved by the Institutional Ethics Committee of the China Academy of Chinese Medical Sciences (IBTCMCACMS21-2109-07).

CRediT authorship contribution statement

Haixia Liu: Data curation, Funding acquisition, Investigation, Writing - original draft, Writing - review & editing. **Zhiyue Chang:** Data curation, Investigation. **Shuling Liu:** Data curation, Investigation. **Ruyuan Zhu:** Data curation, Investigation. **Jiayi Ma:** Data curation, Investigation. **Xinyue Lu:** Data curation, Investigation. **Lei Li:** Data curation, Investigation, Validation, Writing - original draft. **Zhiguo Zhang:** Conceptualization, Funding acquisition, Validation, Writing - original draft.

Declaration of competing interest

The authors declare that they have no known competing financial interests or personal relationships that could have appeared to influence the work reported in this paper.

Abbreviations

AMPK	AMP-dependent protein kinase
BMD	Bone mineral density
BS/TV	Bone surface density
BV/TV	Percent bone volume
ELISA	Enzyme-linked immunosorbent assay
EV	Estradiol valerate
hADSCs	Human adipose-derived stem cells
H&E	Hematoxylin-eosin
IHC	Immunohistochemical
LDL-C	Low-density lipoprotein cholesterol
MEDAG	Mesenteric estrogen-dependent adipogenesis
OP	Osteoporosis
OVX	Ovariectomized
PF	Paeoniflorin
PPARγ	Peroxisome proliferation-activated receptors γ
ROI	Reconstruction area of interest
RT-qPCR	Quantitative real-time polymerase chain reaction
Sham	Sham operation
SMI	Structure model index
Tb.N	Trabecular number
Tb.Sp	Trabecular separation
TC	Total cholesterol
TG	Triglycerides

Appendix A. Supplementary data

Supplementary data to this article can be found online at https://doi.org/10.1016/j.heliyon.2024.e24241.

References

[1] R. Nuti, et al., Guidelines for the management of osteoporosis and fragility fractures, Intern Emerg Med 14 (1) (2019) 85–102.
[2] S. Razmjou, et al., Body composition, cardiometabolic risk factors, physical activity, and inflammatory markers in premenopausal women after a 10-year follow-up: a MONET study, Menopause 25 (1) (2018) 89–97.
[3] H. Zhang, X. Chen, M.R. Sairam, Novel genes of visceral adiposity: identification of mouse and human mesenteric estrogen-dependent adipose (MEDA)-4 gene and its adipogenic function, Endocrinology 153 (6) (2012) 2665–2676.
[4] J.C. Chang, et al., Global molecular changes in a tibial compression induced ACL rupture model of post-traumatic osteoarthritis, J. Orthop. Res. 35 (3) (2017) 474–485.
[5] J. Yang, P. Yu, Identification of MEDAG as a hub candidate gene in the onset and progression of type 2 diabetes mellitus by comprehensive bioinformatics analysis, BioMed Res. Int. 2021 (2021) 3947350.
[6] Z. Li, et al., MEDAG enhances breast cancer progression and reduces epirubicin sensitivity through the AKT/AMPK/mTOR pathway, Cell Death Dis. 12 (1) (2021) 97.
[7] Y. Song, et al., Evaluation of MEDAG gene expression in papillary thyroid microcarcinoma: associations with histological features, regional lymph node metastasis and prognosis, Sci. Rep. 9 (1) (2019) 5800.
[8] S. Li, N. He, L. Wang, Efficiently anti-obesity effects of unsaturated alginate oligosaccharides (UAOS) in high-fat diet (HFD)-Fed mice, Mar. Drugs 17 (9) (2019).
[9] S.C. Chen, et al., Metformin suppresses adipogenesis through both AMP-activated protein kinase (AMPK)-dependent and AMPK-independent mechanisms, Mol. Cell. Endocrinol. 440 (2017) 57–68.
[10] M. Adil, et al., Pioglitazone-induced bone loss in diabetic rats and its amelioration by berberine: a portrait of molecular crosstalk, Biomed. Pharmacother. 94 (2017) 1010–1019.
[11] L.A. Stechschulte, et al., PPARG post-translational modifications regulate bone formation and bone resorption, EBioMedicine 10 (2016) 174–184.
[12] S. Baroi, et al., PPARG in osteocytes controls sclerostin expression, bone mass, marrow adiposity and mediates TZD-induced bone loss, Bone 147 (2021) 115913.
[13] X. Feng, et al., The influence of tetracycline inducible targeting rat PPARgamma gene silencing on the osteogenic and adipogenic differentiation of bone marrow stromal cells, Curr. Pharmaceut. Des. 22 (41) (2016) 6330–6338.
[14] H. Liu, et al., Paeoniflorin inhibits lipopolysaccharide-induced inflammation in LO2 cells by regulating RhoA/NLRP3 pathway, Journal of Traditional Chinese Medical Sciences 8 (2) (2021) 161–165.
[15] Y. Wang, et al., Beneficial effects of paeoniflorin on osteoporosis induced by high-carbohydrate, high-fat diet-associated hyperlipidemia in vivo, Biochem. Biophys. Res. Commun. 498 (4) (2018) 981–987.
[16] Y. Jing, et al., Liuwei Dihuang soft capsules attenuates endothelial cell apoptosis to prevent atherosclerosis through GPR30-mediated regulation in ovariectomized ApoE-deficient mice, J. Ethnopharmacol. 208 (2017) 185–198.
[17] J.R. Ge, et al., Liuwei Dihuang pill ( ) treats postmenopausal osteoporosis with shen (kidney) yin deficiency via janus kinase/signal transducer and activator of transcription signal pathway by up-regulating cardiotrophin-like cytokine factor 1 expression, Chin. J. Integr. Med. 24 (6) (2018) 415–422.
[18] P.H. Yen, et al., A new monoterpene glycoside from the roots of Paeonia lactiflora increases the differentiation of osteoblastic MC3T3-E1 cells, Arch Pharm. Res. (Seoul) 30 (10) (2007) 1179–1185.
[19] Y. Wang, et al., Paeoniflorin regulates osteoclastogenesis and osteoblastogenesis via manipulating NF-kappaB signaling pathway both in vitro and in vivo, Oncotarget 9 (7) (2018) 7372–7388.
[20] W. Guo, et al., The effects and mechanism of paeoniflorin in promoting osteogenic differentiation of MC3T3-E1, J. Orthop. Surg. Res. 17 (1) (2022) 90.
[21] L. Yang, et al., Paeoniflorin attenuates dexamethasone-induced apoptosis of osteoblast cells and promotes bone formation via regulating AKT/mTOR/Autophagy signaling pathway, Evid Based Complement Alternat Med 2021 (2021) 6623464.
[22] Y.X. Zhou, et al., A review on the pharmacokinetics of paeoniflorin and its anti-inflammatory and immunomodulatory effects, Biomed. Pharmacother. 130 (2020) 110505.
[23] J. Ni, et al., Protective effects of paeoniflorin on alveolar bone resorption and soft-tissue breakdown in experimental periodontitis, J. Periodontal. Res. 51 (2) (2016) 257–264.
[24] H. Huang, et al., Paeoniflorin improves menopause depression in ovariectomized rats under chronic unpredictable mild stress, Int. J. Clin. Exp. Med. 8 (4) (2015) 5103–5111.
[25] Y. lIyu, et al., Experimental study on the effect of paeoniflorin in promoting osteogenic differentiation and anti-osteoporosis in mice, Chin. J. Osteoporos. 26 (12) (2020), 1742-1748+1759.
[26] Z. Li, D. Li, X. Chen, Paeoniflorin inhibits receptor activator for nuclear factor kappaB (RANK) ligand-induced osteoclast differentiation in vitro and particle-induced osteolysis in vivo, Med Sci Monit 24 (2018) 1044–1053.
[27] A.B.M. Rabie, J.K. Ho, The mechanism of action of Lipiburn on fat metabolism, Front Biosci (Landmark Ed) 24 (3) (2019) 427–434.
[28] L. Zhang, et al., Association of dyslipidaemia with osteoporosis in postmenopausal women, J. Int. Med. Res. 49 (3) (2021) 300060521999555.
[29] N.I. Papachristou, et al., High-density lipoprotein (HDL) metabolism and bone mass, J. Endocrinol. 233 (2) (2017) R95–R107.
[30] G.H. Li, et al., Positive effects of low LDL-C and statins on bone mineral density: an integrated epidemiological observation analysis and Mendelian randomization study, Int. J. Epidemiol. 49 (4) (2020) 1221–1235.
[31] G. Yubo, et al., Effects of water extract from Ligustri Lucidi Fructus on bone structure and metabolism in ovariectomized rats, Chin. Tradit. Herb. Drugs 47 (7) (2016) 1155–1162.
[32] F. Zhang, et al., Anti-osteoporosis activity of Sanguinarine in preosteoblast MC3T3-E1 cells and an ovariectomized rat model, J. Cell. Physiol. 233 (6) (2018) 4626–4633.
[33] Z. Li, et al., Glycyrrhizin suppresses RANKL-induced osteoclastogenesis and oxidative stress through inhibiting NF-kappaB and MAPK and activating AMPK/Nrf2, Calcif. Tissue Int. 103 (3) (2018) 324–337.
[34] F. Karadeniz, et al., 3,5-dicaffeoyl-epi-quinic acid from Atriplex gmelinii enhances the osteoblast differentiation of bone marrow-derived human mesenchymal stromal cells via WnT/BMP signaling and suppresses adipocyte differentiation via AMPK activation, Phytomedicine 71 (2020) 153225.
[35] G.S. Shen, et al., The GDF11-FTO-PPARgamma axis controls the shift of osteoporotic MSC fate to adipocyte and inhibits bone formation during osteoporosis, Biochim. Biophys. Acta, Mol. Basis Dis. 1864 (12) (2018) 3644–3654.
[36] J.J. Cao, et al., Deficiency of PPARgamma in bone marrow stromal cells does not prevent high-fat diet-induced bone deterioration in mice, J. Nutr. 151 (9) (2021) 2697–2704.